COHERENT INSTABILITIES AT THE FNAL BOOSTER*

V. Lebedev#, A. Burov, W. Pellico, X. Yang, FNAL, Batavia, IL 60510, U.S.A.

Abstract

This paper presents results of experimental and theoretical investigations of transverse beam stability at injection to Fermilab Booster and discuses a novel scheme for transition crossing allowing to avoid the longitudinal emittance growth related to the transition. At reduced chromaticity a multibunch high order head-tail mode develops with growth time of 12 turns at fractional part of tune close to zero. An estimate of the growth rate based on known sources of impedance results in significantly smaller value and cannot explain observed instability growth rate.

INTRODUCTION

Booster [1] is a fast cycling proton synchrotron operating at 15 Hz. To exclude the eddy currents excited in the vacuum chamber by fast changing magnetic field its vacuum chamber is formed by poles of laminated combined function dipoles. That creates large contributions to transverse and longitudinal impedances affecting both transverse and longitudinal beam stability. Presently, transverse instabilities are suppressed by large chromaticity, which negatively affects the dynamic aperture and the beam lifetime. Earlier attempts to stabilize the instability by transverse feedback system were unsuccessful. This paper presents results of studies aimed to understand mechanisms of instability at injection. It also discusses the beam dynamics at the transition crossing and considers a novel scheme allowing one to suppress the longitudinal emittance growth at transition. Main Booster parameters are presented in Table 1.

1. BEAM DYNAMICS AT INJECTION

The instability was evoked by reducing both vertical and horizontal chromaticities. This caused instability in both planes and partial beam intensity loss started at turn 150 after injection. Four channel digital scope running with sampling time of 0.4 ns recorded beam signals of horizontal and vertical beam position monitors (BPM) with 15 cm long plates. Total recording time of 1.6 ms represents ~700 turns. To maximize the resolution for transverse beam motion the signals of two BPM plates for each BPM were combined at a wide band hybrid making the sum and difference signals. The measurements were performed for nominal and half of nominal beam intensities. Off-line treatment of the data included marking boundaries for each bunch, subtracting bunch offsets from the differential signal, and integrating bunch signals to obtain the density and dipole moment distributions. The following bunch parameters were computed for each bunch: AC bunch intensity, longitudinal and transverse centers of gravity, rms bunch length and transverse dipole moments. Note that the relative revolution frequency change during the first 200 turns is about 10^{-3}, and needs to be taken into account when bunch boundaries are marked. Beam positions (offsets) are also changing fast and they were corrected for each turn.

Table 1: Booster parameters

Energy	0.4 – 8 GeV
Transition energy	5.1 GeV
Total number of particles	$4.5\cdot10^{12}$
Circumference	474.2 m
Harmonic number, q	84
Betatron tunes, Q_x/Q_y	6.82 /6.81
RF voltage	0.7- 0.9 MV
Injection type	H^-, 10 turns

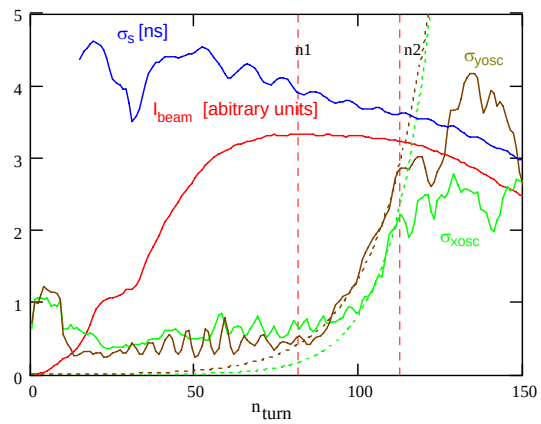

Figure 1: Changes of beam parameters during first 150 turns; red line – AC beam intensity, blue line – rms bunch length, vertical (brown line) and horizontal (green line) rms transverse dipole moments. Dotted lines present exponential fits to the rms dipole moments inside a bunch. All signals are averaged over all 84 bunches; beam intensity - $4.5\cdot10^{12}$.

The following sequence of actions happens during injection (see Figure 1). First, injection orbit bump is created just before injection. Then, the linac beam is injected during 5 or 10 turns for half or full beam intensity, respectively. When the injection is finished the orbit bump is switched off (it takes 10-20 turns) and RF voltage is adiabatically increased causing beam to be bunched at turn 70 with RF voltage continuing to grow. The first sign of the instability appears at turn 80 causing the beam intensity drop at turn 150.

An accurate knowledge of betatron and synchrotron tunes is important to understand the nature of the instability. Small oscillations excited by injection process were helpful to determine the tunes. Figure 2 presents turn-by-turn vertical positions for all 84 bunches and corresponding spectrum. Although betatron motion decays fast the direct fitting by exponentially decaying

* Work supported by the U.S. Department of Energy under contract No. DE-AC02-76CH03000
#val@fnal.gov

sinusoid allowed us to determine the fractional part of tune with three digits accuracy. The decay time is used to estimate the lattice chromaticity (see below). To determine the synchrotron tune we analyzed the frequency of quadrupole synchrotron oscillations excited in the course of beam bunching. They are clearly visible on the rms bunch length presented in Figure 1. The synchrotron tune at turns 50 to 120 grows from 0.03 to 0.06 in accordance with expectations. Because of beam loading and beam space charge the synchrotron tune dependence on time varies with beam intensity. Tables 2 and 3 summarize results of measurements.

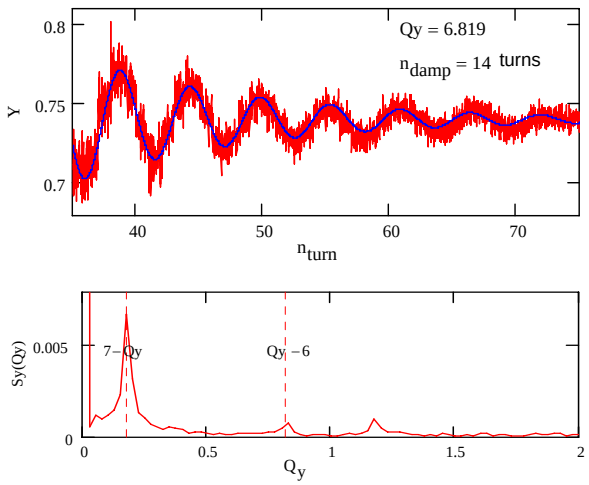

Figure 2: Dependence of vertical bunch-by-bunch positions excited by injection process on turn number and corresponding spectrum; beam intensity $4.5\cdot10^{12}$.

Table 2: Results of measurements of tunes and damping times at turns 30 to 60

Number of particles	$2.3\cdot10^{12}$	$4.5\cdot10^{12}$
Horizontal tune, Q_x	6.830	6.825
Vertical tune, Q_y	6.831	6.819
X-plane decoherence time, turns	15	13
Y-plane decoherence time, turns	18	16

Knowing synchrotron tune and longitudinal density distribution one can obtain the longitudinal distribution function. Fitting to the data of turn 69 corresponding to the end of bunching process yields (see Figure 3):

$$f(I) = \frac{2}{C}\left(1 - \frac{E(I)}{E_{\max}}\right) \quad , \tag{1}$$

where

$$E = \frac{\dot{\phi}^2}{2} + \Omega_s^{\,2}\left(1 - \cos\phi\right) \quad , \qquad E_{\max} = 2\Omega_s^{\,2} \quad , \quad C = \int_0^{I(E_{\max})} f\left(E(I)\right) dI \quad , \tag{2}$$

$\phi \in [-\pi, \pi]$ is the longitudinal coordinate inside RF bucket, and Ω_s is the synchrotron frequency. Corresponding longitudinal emittance (area in the phase space including 100% particles) is 0.06 eV·s per bunch.

The measurement results clearly demonstrate that the instability does not develop before bunches are formed; but when it finally starts it looks rather unusual: the dipole moment distribution for all bunches on nearby turns exhibits almost the same pattern only slowly moving in the direction opposite to the beam direction as shown in Figure 4. Note that although the data are presented for every 5-th turn the distributions for missed turns are monotonically changing between the data for presented turns. Such behavior corresponds to the head-tail instability developing at tunes equal to $Q_{x,y} - 7 + 3Q_s$. Their values are close to zero (see Table 3). At full beam intensity the horizontal motion in the bunch tail is larger than in the head pointing out that the horizontal instability is the strong head-tail instability. Therefore data for half of nominal intensity, where the head-tail is weak, were used for impedance estimates considered below.

Table 3: Results of measurements of instability growth times and synchrotron tune

Number of particles	$2.3\cdot10^{12}$	$4.5\cdot10^{12}$
Synchrotron tune, Q_s at turn 100	0.047	0.057
$\Delta Q_x = Q_x - 7 + 3Q_s$	–0.029	–0.004
$\Delta Q_y = Q_y - 7 + 3Q_s$	–0.028	–0.010
X instability growth time, turns	18	12
Y instability growth time, turns	14	14

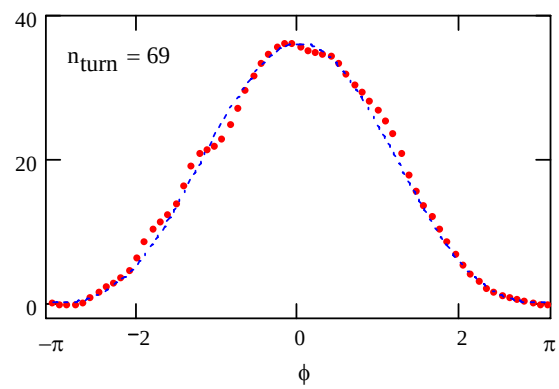

Figure 3: Measured (red dots) and fitted (blue dashed line) longitudinal density distribution at turn 69; beam intensity $4.5\cdot10^{12}$.

2. CHROMATICITY ESTIMATE

Beam decoherence at turns 30 to 60 allows one to make an estimate of chromaticities. Neglecting the effect of impedance on the beam stability and that the beam is partially bunched one can write the damping rate as:

$$n._{decoh}^{\;-1} \approx \left|\xi - n\eta\right| \sigma_{\Delta p/p} \quad , \tag{3}$$

where $\eta = \alpha - 1/\gamma^2$ is the slip factor ($\eta = -0.458$ at injection), ξ is the chromaticity and n is the mode number determined so that the lab-frame betatron frequency is:

$$\omega_n \approx \omega_0\left(Q + n\right) \quad . \tag{4}$$

For data presented in Table 2, $n = -7$ and one can neglect $n\eta$ in comparison with ξ. This yields for absolute values of chromaticities: $|\xi_x| \approx 85$ and $|\xi_y| \approx 70$. As will be seen later the real part of transverse impedance at this frequency is sufficiently small and does not make significant correction for chromaticities.

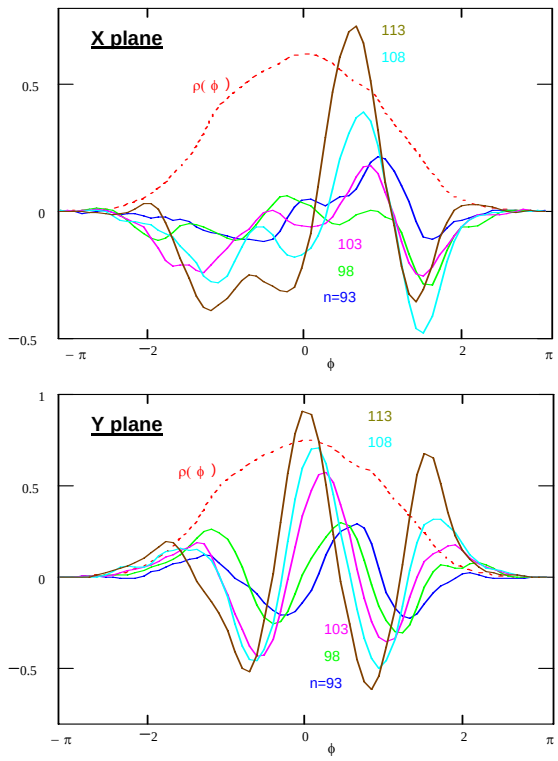

Figure 4: Measured dipole moment distributions for *x*-(top) and *y*-planes (bottom) over bunch length for every 5-th turn (turns from 93 to 113); beam intensity $4.5\cdot10^{12}$.

The signs of chromaticities can be determined from the direction of head-tail wave propagation (see Figure 4). In the case of weak head-tail effect the "air-bag" model yields that the dependence of average transverse position along the bunch is [2]:

$$\bar{x}(t,s) = x_0 \cos\left(\Delta Q\omega_0 t - \kappa\frac{s}{L_b} + \psi\right)\cos\left(m\,\mathrm{acos}\frac{s}{L_b}\right) \quad , \tag{5}$$

where $\Delta Q = Q + n + mQ_s$ is the mode tune, $\kappa = \xi L_b / \eta R_0$ is the head-tail phase, L_b is the bunch length, R_0 is the machine radius, m is the synchro-betatron mode number and ψ is an arbitrary phase. Eq. (5) yields that the velocity of the head-tail wave is:

$$\frac{d}{dt}\left(\frac{s}{L_b}\right) = \frac{\Delta Q\omega_0}{\kappa} \quad . \tag{6}$$

The mode tunes for parameters of our experiment are presented in Table 2. Data for $2.3\cdot10^{12}$ particles (where the weak head-tail approximation is better applicable) were used to estimate the chromaticity. The betatron wave velocities are $d(\Delta s/L_b)/dt \approx -0.022$ and -0.025 turn^{-1}, correspondingly, for *x* and *y*-planes. That yields the head-tail phases: $\kappa_x \approx 8$ and $\kappa_y \approx 7$ and the negative signs of both chromaticities. Described above chromaticity measurements yields ~2 times smaller values for $\kappa_{x,y}$ if L_b equal to one forth of full bucket length is used. Discrepancy is apparently related to the poor accuracy of ΔQ, which small value is obtained as difference of two large numbers, and insufficient accuracy of Eq. (5) ignoring particle interaction and bunch structure.

3. INSTABILITY GROWTH RATE

To estimate the instability growth rate for bunched beam we use the "air-bag" model [2]. For weak head-tail interaction it yields that the complex betatron tune shift is:

$$\delta Q_{n,m} = \frac{iI_0 R_0 Z_{\perp eff\ n,m}}{4\pi\left(mc^2/e\right)\gamma\beta^2 Q} \quad , \tag{7}$$

where

$$Z_{\perp eff\ n,m} = \sum_{k=-\infty}^{\infty} Z_\perp(\omega_k)\left(\mathrm{J}_m\left(\frac{\omega_k L_b}{\beta c} - \kappa\right)\right)^2 \quad , \tag{8}$$

where I_0 is the beam current, c is the speed of light, m and e are the particle mass and charge, γ and β are its relativistic factors, $Z_\perp(\omega)$ and R_0 are the ring impedance and average radius, $\omega_k = \omega_0\left(Q + n + mQ_s + kN_b\right)$, and N_b is the number of bunches which for Booster coincides with harmonic number q. Taking into account that the instability growth rate per turn is $\lambda_{n,m} = -2\pi\,\mathrm{Im}(\delta Q)$, and that for observed instability n = -7 and m = 3, and using instability growth rates for $2.3\cdot10^{12}$ particles from Table 3 one obtains the effective impedances to be: $\mathrm{Re}(Z_{Xeff\ -7,3})$ = 43 MΩ/m, $\mathrm{Re}(Z_{Yeff\ -7,3})$ = 55 MΩ/m.

The imaginary part of impedance can be found from tune dependence on the beam intensity presented in Table 2. At that time the beam is not completely bunched and one can use the continuous beam approximation to estimate the impedance. In this case the tune shifts for horizontal and vertical betatron motions are [3]:

$$\begin{bmatrix}\delta Q_x \\ \delta Q_y\end{bmatrix}_n = -\frac{I_0 R_0}{4\pi\left(mc^2/e\right)\gamma\beta^2 Q}\begin{cases}\mathrm{Im}\left(Z_X(\omega_n) - Z_D(0)\right) & , \\ \mathrm{Im}\left(Z_Y(\omega_n) + Z_D(0)\right) & ,\end{cases} \tag{9}$$

where $Z_D(\omega)$ is the detuning impedance (Fourier transform of the detuning wake). For n = -7 that yields: $\mathrm{Im}(Z_X(\omega_{-7})-Z_D(0))$ = 24 MΩ/m and $\mathrm{Im}(Z_Y(\omega_{-7})+ Z_D(0))$ = 58 MΩ/m, where ω_{-7}=76 kHz. Earlier measurements [4] with beam motion excited by the vertical kicker yielded very close value for the vertical tune shift. The horizontal tune shift was not measured. Note that in distinction from measurements presented here, the kicker measurements excite many multi-bunch modes while BPMs report a single beam position per turn combined from unknown weighted sum of bunch signals. Thus, the frequency at which the response is measured is not well determined.

4. TRANSVERSE BOOSTER IMPEDANCE

In the first approximation we can consider that the Booster impedance is formed from two major contributions coming from the round stainless steel vacuum chamber and the laminated dipoles.

The impedance per unit length of round vacuum chamber with thin wall was computed in Ref. [5]. The result is:

$$Z_{L\perp} = \frac{iZ_0}{2\pi a^2\beta}\left[\frac{2\beta^2\left(e^{kd}(1+kb) - e^{-kd}(1-kb)\right)}{e^{kd}(1+ka)(1+kb) - e^{-kd}(1-ka)(1-kb)} + \frac{1}{\gamma^2}\right]. \tag{10}$$

where a and b are the inner and outer radii of vacuum chamber, $d \equiv b-a \ll a$ is its thickness, $k = (1+i)/\delta$,

$\delta = c/\sqrt{2\pi\sigma\omega}$ is the skin depth, and $Z_0 = 4\pi/c \approx 377\,\Omega$ is the impedance of free space. The total length of such vacuum chamber is 197 m, a=43 mm, and d_0=1.6 mm. Figure 5 shows corresponding contribution to the impedance. As one can see its real part achieves maximum at 3 kHz where $\delta \approx \sqrt{ad}$. Its value does not depend on the vacuum chamber conductivity and is:

$$\mathrm{Re}(Z_{L\perp})\big|_{\max} \approx \frac{iZ_0\beta}{4\pi a^2} \quad . \tag{11}$$

The imaginary part of impedance achieves its maximum at zero frequency where it is determined by pure electrostatic beam interaction with vacuum chamber.

Computation of the impedance for laminated vacuum chamber in the entire frequency range is a complicated problem and as far as we know has not been solved. Before we consider it let us discuss the impedance of flat vacuum chamber manufactured from non-laminated steel. As follows from results of Ref. [6] the horizontal and vertical impedances per unit length are:

$$Z_{Lx} = i\frac{Z_0}{2\pi a^2\beta}\left[\frac{\pi^2}{24} + \beta^2\int_0^\infty \frac{(u-ka/\mu)\exp(-u)u\,du}{k\cosh(u)+u\sinh(u)}\right] \quad , \tag{12}$$

$$Z_{Ly} = i\frac{Z_0}{2\pi a^2\beta}\left[\frac{\pi^2}{12} + \beta^2\int_0^\infty \frac{(u-ka/\mu)\exp(-u)u\,du}{k\sinh(u)+u\cosh(u)}\right] \quad ,$$

where the vacuum chamber is assumed to be confined by two infinite magnetic blocks filling upper and lower half spaces and separated by distance $2a$, μ is the magnetic permeability, and similarly to the round vacuum chamber $k = (1+i)/\delta$ and $\delta = c/\sqrt{2\pi\sigma\omega\mu}$. There are two types of dipoles: focusing and defocusing. The summed length of each type is 139 m, and the half-gaps are 20.8 and 28.5 mm, respectively. Figure 5 shows corresponding contributions to the impedances. As one can see the real parts of both impedances achieve maximum at ~100 kHz (where $\mu\delta \approx a$). Their values do not depend on vacuum chamber conductivity and μ. They are:

$$\mathrm{Re}\begin{bmatrix} Z_{Lx} \\ Z_{Ly} \end{bmatrix}\Bigg|_{\max} \approx \frac{iZ_0\beta}{4\pi a^2}\begin{cases} 0.336\,, & a/\mu\delta \approx 0.372, \\ 0.5\,, & a/\mu\delta \approx 0.89. \end{cases} \tag{13}$$

With frequency decrease, both impedances decrease and approach zero at zero frequency. The reason of impedance decrease at small frequencies is related to the increase of skin depth with subsequent magnetic flux "shortening" by the wall magnetism; so that the tangential component of beam magnetic field is diminishing. That causes decrease of currents excited in the vacuum chamber, and, consequently, decreases power loss and impedance. Note that the real parts of impedances for the round thin wall and flat magnetic vacuum chambers achieve almost the same maximum value. Actually, the smaller value for flat vacuum chamber is related to its more open geometry than to its magnetism. This is a manifestation of more general law which limits the absolute value of wide-band transverse impedance so that $|Z_{L\perp}|_{\max} \le Z_0/(2\pi a^2\beta)$ (see "careless limit" in Ref. [2]).

To make an estimate of impedance introduced by laminated dipoles we take into account that for the given skin depth both the resistance and the magnetic conductivity of vacuum chamber per unit length are increased by factor $2a/d_{lam}$ where d_{lam} is the lamination thickness. That results in that the horizontal and vertical impedances can be approximated by Eq. (12) where ka/μ need to be replaced by $kd_{lam}/2\mu$. At high frequencies this result coincides with the result obtained in Ref. [7].

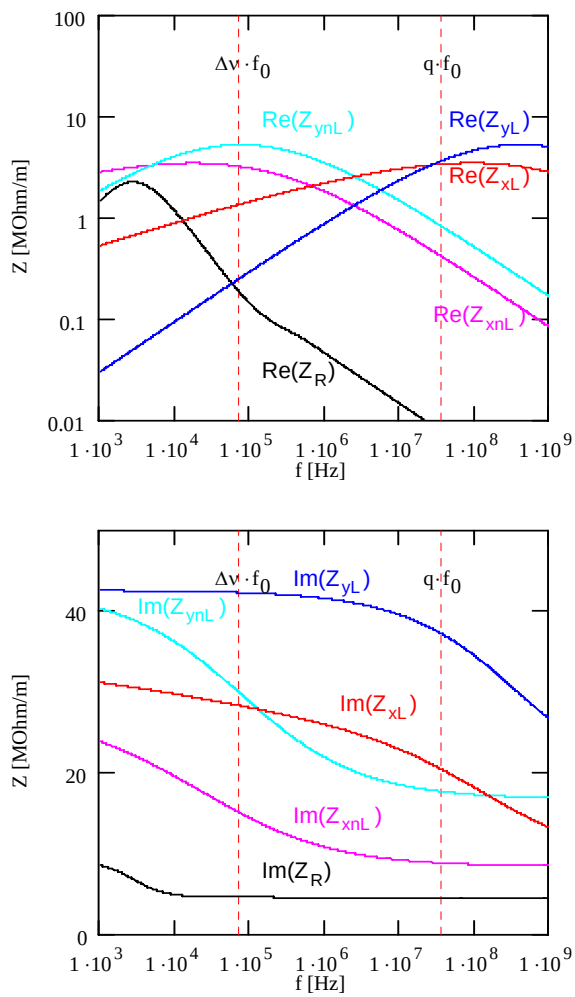

Figure 5: Contributions to the real (top) and imaginary (bottom) parts of impedance from different pieces of vacuum chamber; Z_R – round vacuum chamber, Z_{xL} and Z_{yL} – laminated dipoles with μ=1000, Z_{xnL} and Z_{ynL} – mark contributions corresponding to non-laminated dipoles.

To get the total ring impedances one needs to sum contributions of round vacuum chamber and focusing and defocusing laminated dipoles with fudge factors accounting the beta-function variation. They are equal to:

$$k = \frac{Q}{2\pi R_0^{\,2}} \oint_{\text{over given type}} \beta(s)ds \quad . \tag{14}$$

Integration over Booster design lattice yields: for focusing dipoles – k_x = 2.64, k_y = 0.65; for defocusing dipoles – k_x =1.00, k_y =1.62; for round vacuum chamber – k_x = 0.64, k_y = 1.82. Figure 6 presents resulting total impedances.

Computation of effective impedances responsible for the tune shift yields: $\mathrm{Im}(Z_X(\omega_{-7})-Z_D(0))$ = 26 MΩ/m and

$\mathrm{Im}(Z_Y(\omega_{-7}) + Z_D(0)) = 85$ MΩ/m. Taking into account that the estimate of impedance for laminated dipoles is rough at small frequencies and the effects of bunching and momentum spread are completely ignored one can conclude that there is a satisfactory agreement with the measurement result presented at the end of Section 2.

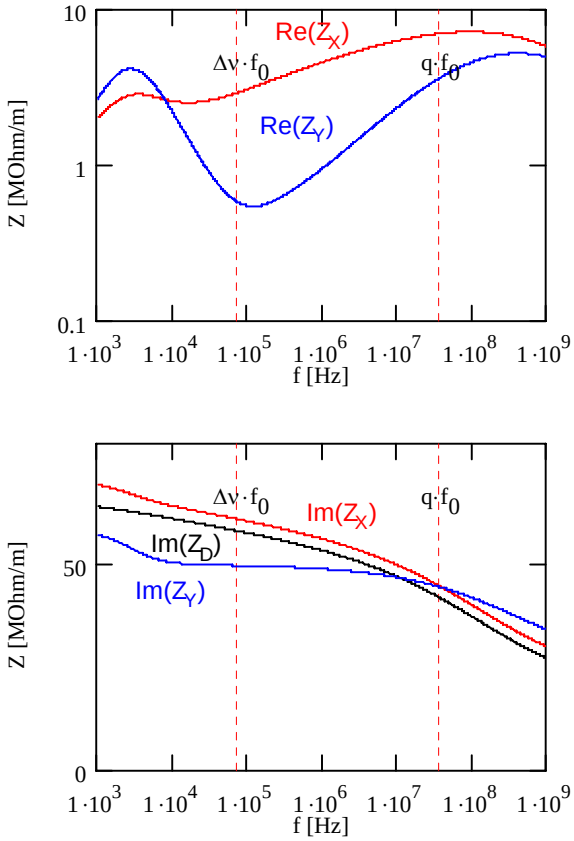

Figure 6: Real (top) and imaginary (bottom) parts of Booster total impedances and imaginary part of detuning impedance.

There is large disagreement in the estimate of real part of impedances. From the experiment we know multi-bunch and head-tail modes ($n = -7$, $m = 3$). That sets frequencies in the sum of Eq. (8) to be $\omega_k/2\pi = -0.012 \pm 37.9k$ MHz. For $\xi \approx -70$ the head-tail phase is $\kappa = 3.4$ and the Bessel function $J_3(\kappa)^2$ is close to its first maximum. That maximizes the contribution for addend with $k = 0$ ($f \approx 12$ kHz). Also note that other contributions coming from positive and negative frequencies ($\pm k$) in Eq. (8) partially cancel each other, thus reducing the sum. The considered above estimate of laminated dipole impedance ignores the plate-to-plate capacitance which reduces the real part of impedance at frequencies above ~500 MHz. μ=1000 is used in the impedance estimate in the entire frequency range. This cannot be correct at high frequencies where μ should be decreasing due to skin depth becoming smaller than the domain size. Therefore a frequency range of 0 to 500 MHz ($k \in$ [-13, 13]) is used to compute the effective impedances of Eq. (8). That results in 6 and 3.2 MΩ/m for horizontal and vertical planes, correspondingly, where contributions coming from zero term (k=0) are 0.37 and 0.55 MΩ/m. Although the model correctly points out that the real part of horizontal impedance is larger than for the vertical one, it predicts the instability growth rates and the real parts of impedances by an order of magnitude smaller than the measured values. The reason of the discrepancy is not clear. It hardly can be explained by underestimation of the impedance for laminated magnets. It is already close to its theoretical maximum in the required frequency range. There is a possibility of unaccounted impedance, but also the instability can be related to the presence of electrons stored in the beam. The residual gas pressure in Booster is about 10^{-7} Torr. That corresponds to the beam space charge compensation time of about 0.1 sec. Although it is too long to make any effect at 200 turns the multipactor discharge can greatly accelerate the production of electrons. Further experimental studies are required to test this possibility.

5. TRANSITION CROSSING WITH RF VOLTAGE JUMP TECHNIQUE

Measurements of beam dynamics at injection were performed similar to the considered above transverse instability measurements. The sum signal of a BPM was digitized with 0.2 ns sampling time. Then, the signal of each bunch was integrated numerically to obtain the particle density along the bunch. Figure 7 presents dependence of bunch length (computed using few different algorithms) on time in vicinity of transition. One can see that the bunch size starts to shrink approximately 0.2 ms after transition and after achieving a minimum blows up. After few synchrotron periods these synchrotron oscillations result in the longitudinal emittance growth.

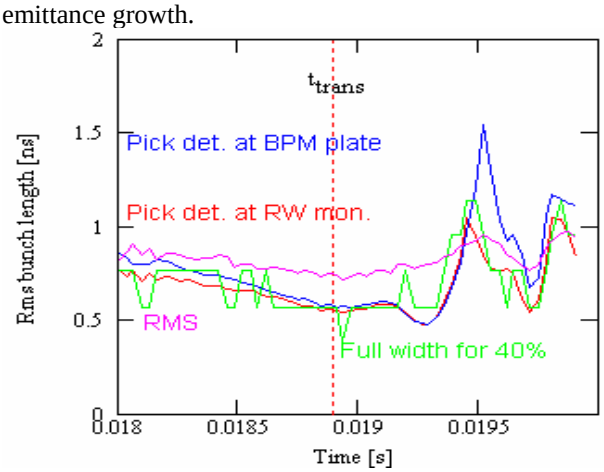

Figure 7: Dependence of bunch length (computed using different methods from measured data) on time in vicinity of transition crossing. Transition time is shown by the vertical line.

Observed longitudinal dynamics is consistent with development of the negative mass instability due to longitudinal space charge force. First, let us consider a simple linear model with a parabolic density distribution

and linearized RF voltage over bunch length. Standard procedure results in a system of differential equations describing evolution of the bunch ellipse in the phase space. The solution was carried out numerically for sinusoidally changing bending field and given dependence of accelerating voltage on time. The solid line on the top picture of Figure 8 presents results of numerical simulation for nominal parameters of transition crossing. One can see close resemblance with measurement results presented in Figure 7. Examination of the solution shows that the sign change of the space charge force from repulsion to attraction after transition crossing causes large amplitude quadrupole synchrotron oscillations. More detailed multi-particle simulations with ESME [8] show that after few synchrotron oscillations they decohere causing longitudinal emittance growth.

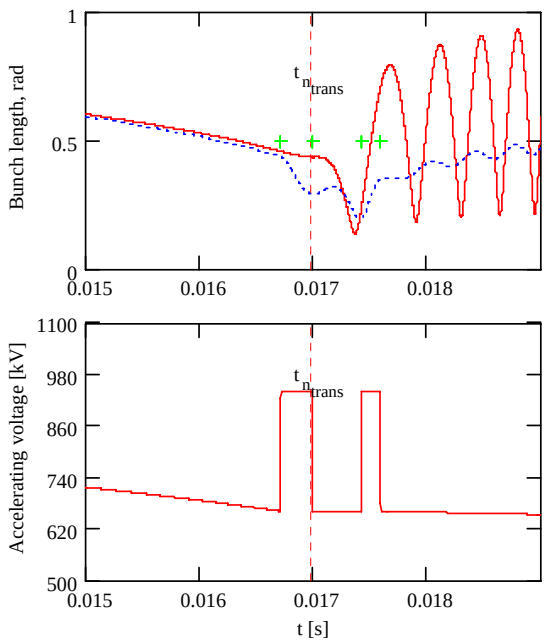

Figure 8: Dependence of bunch length (top picture) on time simulated in linear model in vicinity of transition crossing: solid line – no fast change in RF voltage, dashed line – RF voltage has two pulses as shown in the bottom picture. Transition time is shown by the vertical line

The following procedure was suggested to prevent a development of such oscillations. Approximately quarter synchrotron period before transition crossing the accelerating voltage is rapidly increased. That causes the bunch to be overfocused. Actually the bunch length changes comparatively little due to small particle mobility at transition but momentum spread in the bunch is strongly amplified. Voltage is returned to its nominal value at transition. The accumulated momentum spread causing bunch shortening before transition is now causing the bunch lengthening which prevents bunch collapse due to space charge force. Using the second smaller voltage pulse after half synchrotron period allows one to suppress synchrotron oscillations after transition as shown by dashed line in Figure 8. Figure 9 shows results of ESME simulations with and without voltage manipulations clearly demonstrating suppression of longitudinal emittance growth.

This method was tested in Booster and demonstrated expected reduction of emittance growth. Its use in operations for a few shifts was also successful. Two hardware problems are pending its permanent use in Booster operations. The first is related to insufficient time resolution of the low level RF timing; and the second one is high sensitivity to RF station loss because Booster RF does not have sufficient voltage excess.

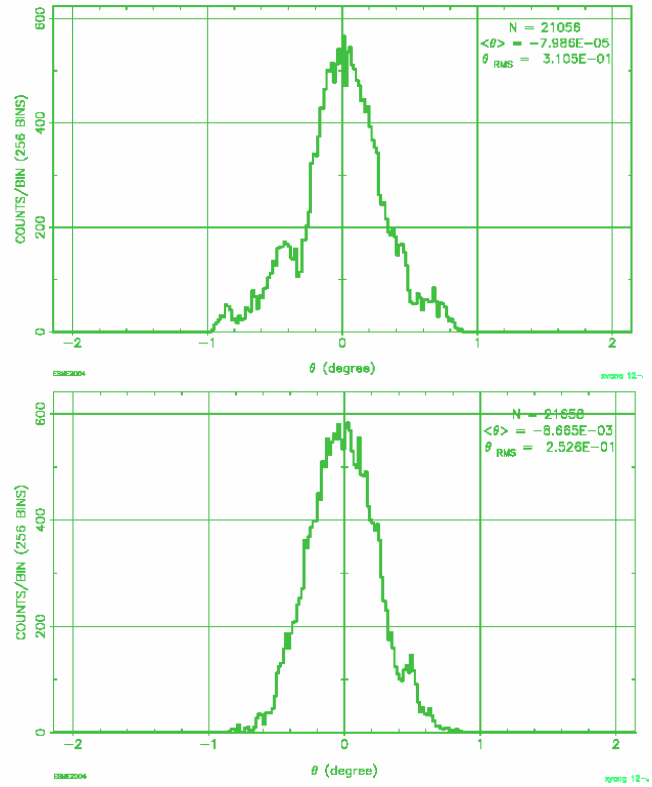

Figure 9: Particle distribution over bunch length at the end of Booster cycle simulated with ESME: top – no RF manipulations, bottom – RF manipulations are on.

REFERENCES

[1] "Booster Synchrotron", edited by E. L. Hubbard, FNAL TM-405, 1973.

[2] A. W. Chao, "Physics of Collective Beam Instabilities," J. Wiley & Sons, Inc, 1993..

[3] A. Burov and V. Danilov, "Suppression of Transverse Bunch Instabilities by Asymmetries in the Chamber geometry.", Phys. Rev. Lett. 82, 2286 (1999)

[4] Huang Xiaobiao, *private communications*, 2005.

[5] A. Burov, V. Lebedev, "Transverse Resistive Wall Impedance for Multi-Layer Round Chambers", p. 1452, EPAC'02

[6] A. Burov, V. Lebedev, "Transverse Resistive Wall Impedance for Multi-Layer Flat Chambers", p. 1452, EPAC'02

[7] A. Burov, V. Danilov, *private communications*, 2002.

[8] J. MacLachlan, "User's Guide to ESME 2002," FNAL, November 2002